Movement of a Loop in Domain 3 of Aerolysin Is Required for Channel Formation†

Jamie Rossjohn,‡,§ Srikumar M. Raja,|| Kim L. Nelson,|| Susanne C. Feil,‡,§ F. Gisou van der Goot,⊥ Michael W. Parker,‡ and J. Thomas Buckley*,||

The Ian Potter Foundation Protein Crystallography Laboratory, St. Vincent's Institute of Medical Research, 41 Victoria Parade, Fitzroy, Victoria 3065, Australia, Département de Biochimie, Université de Genève, 30 quai E. Ansermet, 1211 Genève, Switzerland, and Department of Biochemistry and Microbiology, University of Victoria, Victoria, British Columbia, Canada V8W 3P6

Received August 25, 1997; Revised Manuscript Received October 20, 1997⊗

ABSTRACT: Aerolysin is a channel-forming toxin that must oligomerize in order to become insertion-competent. Modeling based on the crystal structure of the proaerolysin dimer and electron microscopic images of the oligomer indicated that a loop in domain 3 must move away from the β-sheet that forms the main body of the protein before oligomerization can proceed. In order to determine if movement actually occurs, strategically located amino acids in the loop and in the sheet were replaced with cysteines by site-directed mutagenesis. A double mutant was produced in which the new cysteines, at position 253 on the loop and position 300 in the sheet, were close enough together to allow formation of a disulfide bridge. The double mutant was unable to oligomerize, and it was completely inactive, showing not only that the bridge had formed but also that movement of the loop was essential for formation of the oligomer. The existence of the bridge was confirmed by X-ray crystallography. The reduced form of the protein and the single mutants T253C and A300C were as active as wild type, indicating that the amino acid replacements themselves had no functional consequences. Labeling studies using an environment-sensitive fluorescent sulfhydryl-reactive probe confirmed that the structure of the protein changes in the loop region as a consequence of proteolytic activation of proaerolysin, a step which also must precede oligomerization.

Proaerolysin is a channel-forming protein toxin precursor secreted by *Aeromonas* spp. In order for it to exert its pore-forming activity, it must first be activated by proteolytic removal of a C-terminal peptide. The aerolysin that is formed can then undergo a transition from a dimeric, water-soluble form to a heptameric complex which is capable of inserting into membranes (reviewed in ref *1*). We have modeled this transition using the crystal structure of the dimeric form and the electron microscopic images of the heptamer bound to lipid vesicles (*2*). The crystal structure indicates that the proaerolysin monomer is bilobal, with domain 3 (residues 179−195, 224−274, 299−310, and 399−409) located in the middle of the large lobe as shown in Figure 1. Domain 3 is a compact globular domain shaped like a box, with the front formed by a five-stranded antiparallel β-sheet of dimensions 20 Å by 35 Å and the back by a long loop that has a small amount of two-stranded sheet (residues 245−246, and 258−259). This domain is quite narrow, with a thickness of only about 20 Å. Modelling based on the electron microscopic images of the oligomer indicates that the five-stranded sheet in domain 3 is involved in oligomeric contacts and that the loop must move to allow these contacts to occur and also to avoid collision with the membrane upon insertion. Alternatively, the loop may be directly involved in formation of the amphipathic β-barrel of the oligomer that transverses the membrane. This latter possibility is suggested by the recently obtained crystal structure of *Staphylococcus aureus* α-hemolysin (*3*), in which a long loop becomes exposed to form the transmembrane β-barrel in the heptameric membrane channel and a comparable loop has been proposed to form the heptameric barrel of anthrax toxin protective antigen (*4*). Regardless of which way the aerolysin oligomer is formed, the long loop in domain 3 must move away from the sheet sometime during the oligomerization process. In order to confirm that loop movement occurs, we decided to engineer a disulfide bridge between the loop and the sheet in domain 3. In addition, the corresponding two single cysteine mutants were generated. We used them in labeling studies with the location-sensitive, sulfhydryl-reactive reagent MIANS[1] to get evidence of movement of the loop as a consequence of trypsin activation of proaerolysin.

† This work was supported by a grant from the Natural Sciences and Engineering Research Council of Canada (J.T.B.). M.W.P. is an Australian Research Council Senior Research Fellow and acknowledges support from the Australian National Health and Medical Research Council.

* Author to whom correspondence should be addressed. Telephone 250-721-7081. FAX: 250-477-0579. E-mail: tbuckley @uvic.ca.

‡ St. Vincent's Institute of Medical Research.

§ These authors contributed equally to the crystallographic aspects of this paper.

|| University of Victoria.

⊥ Université de Genève.

⊗ Abstract published in *Advance ACS Abstracts,* December 1, 1997.

[1] Abbreviations: MIANS, 2-(4-maleimidoanilino)naphthalene-6-sulfonic acid, sodium salt; HEPES, *N*-(2-hydroxyethyl)piperazine-*N*′-2-ethanesulfonic acid; Tris, tris(hydroxymethyl)aminomethane; DTT, dithiothreitol; SDS−PAGE, sodium dodecyl sulfate−polyacrylamide gel electrophoresis.

S0006-2960(97)02103-X CCC: $15.00
Published on Web 01/13/1998

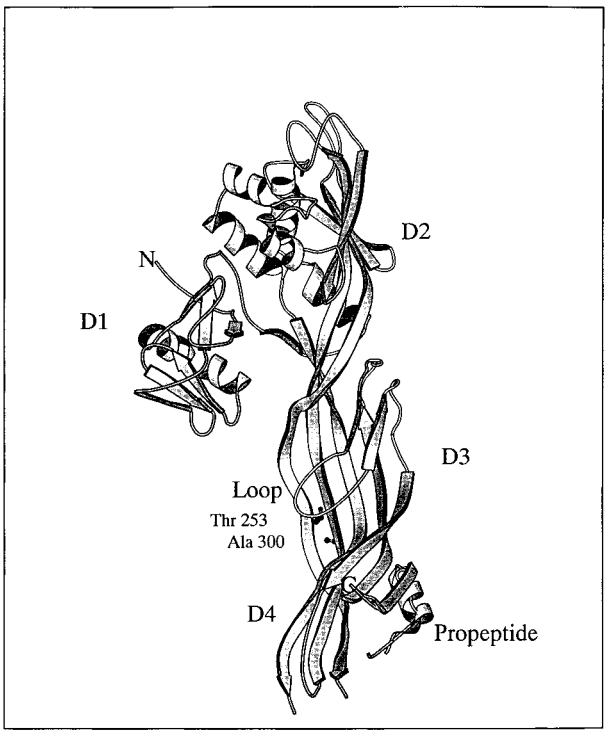

FIGURE 1: Cartoon representation of the chain fold of the proaerolysin dimer showing the position of mutations discussed in the text. The domains are labeled D1−D4, and the sites of mutation are designated in ball-and-stick fashion. This figure was produced using the program MOLSCRIPT (*21*).

EXPERIMENTAL PROCEDURES

Design of Mutants. Potential sites for cysteine residue pairs that might form disulfide bonds were selected using the method of Hazes and Dijkstra (*5*). Briefly, potential residue pairs were initially identified on the basis of appropriate Cβ−Cβ distances. Sulfur positions were generated for these residues, and a check was made to determine if certain stereochemical criteria were obeyed. An important criterion was that the χ^{-3} angles of a potential bridge should not deviate by more than 30° from observed preferences. Selected pairs were subjected to energy minimization, and energetically favorable conformations were chosen (less than 10 kcal/mol). The success of this method relies on the assumption that main-chain conformations are very similar between wild-type and mutant. Calculations were based on the recently refined model of proaerolysin (ref *2*; PDB code is 1PRE). The model had been refined to an *R*-factor of 0.206 at 2.8 Å resolution with good stereochemistry. The best candidate for engineering a disulfide bridge between the loop and sheet of Domain 3 was the residue pair of Thr 253 and Ala 300 (Figure 1). We predicted that the two residues would form a bond that would comply with the stereochemical (χ^{-3} approximately 90.0°) and conformational energy (0.9 kcal/mol) criteria.

Site-Directed Mutagenesis. Individual amino acids were replaced with cysteines by site-directed mutagenesis of either the 715 bp *Hin*dIII−*Hin*cII or the 975 bp *Hin*cII−*Eco*RI portion of *aerA* in the phagemid pTZ18U, using procedures we have described previously (*6*, *7*). Changes were confirmed by DNA sequencing using Sequenase version 2 and materials and procedures provided by U. S. Biochemicals. Once a clone was identified, the DNA was inserted into pMMB66HE in frame with the rest of *aerA* and transferred to *Aeromonas salmonicida* strain CB3 by conjugative mating as described earlier (*8*). This strain was used for production of each of the mutant proaerolysins and for purification according to our published methods (*9*).

Crystallization and Data Collection. All of the mutants ran as single bands on SDS−PAGE. They were crystallized using the hanging drop vapor diffusion method under conditions similar to those we used for the wild-type protein (*10*). Optimal crystallization conditions varied somewhat for each mutant. For the A300C mutant, the protein concentration was 1.8 mg/mL in 20 mM HEPES, pH 7.4, and 150 mM NaCl. For the T253C mutant, it was 2.0 mg/mL in 20 mM Tris-HCl, pH 8.0. For the double mutant T253C/A300C, the protein concentration was 2.2 mg/mL in 20 mM Tris-HCl, pH 7.4. The precipitant for all mutant proteins was 15% w/w PEG 4000, 100 mM sodium acetate, pH 5.6. Crystal size was improved by a combination of streak-seeding and macro-seeding. All the mutant crystals were found to be isomorphous to the wild-type ones (under cryo-cooling conditions of 100 K) with maximal deviations of cell constants of less than 0.5% from the native values. They all belonged to the space group $P4_32_12$ and contained a dimer in the asymmetric unit of the unit cell.

The X-ray diffraction data were collected using a MAR-Research area detector with CuK_α X-rays generated by a Rigaku RU-200 rotating-anode X-ray generator. All data were collected at 100 K using an Oxford Cryosystems Cryostream Cooler. Prior to flash−freezing, the crystals were transferred into artificial mother liquor containing glycerol with stepwise increases (5% increments at 5 min intervals) in glycerol content until a level of 25% was obtained. The diffraction data were processed and analyzed using programs in the HKL (*11*) and CCP4 suites (*12*). The relevant data statistics are presented in Table 1.

Structure Solution and Refinement. The mutant structures were determined using the wild-type model. This model has a crystallographic *R*-factor of 22.1% and a free *R*-factor of 28.7% for all data to 2.3 Å resolution, and it exhibits excellent stereochemistry (ref *2* and unpublished results). Refinement began with the wild-type model which had solvent molecules removed. Rigid-body refinement in XPLOR version 3.1 (*13*) was used to compensate for any possible changes in crystal packing. As the asymmetric unit of the crystal contained two proaerolysin monomers, attempts were made to introduce noncrystallographic symmetry restraints in various ways. However, this always resulted in increases in the R_{free} value and hence was not pursued. This is not surprising as a detailed analysis of the wild-type crystal structure demonstrates that the monomers do not superimpose well because of crystal packing forces (unpublished results). All models were refined using grouped *B*-factors, where each secondary structure element or loop was treated as one group and bulk solvent corrections were employed. Difference Fourier maps indicated the positions of solvent atoms and suggested various minor changes to the backbone structure as well as placement of side-chain atoms. Solvent atoms were only accepted if they appeared as peaks with signals of more than 4 times the rms error in the difference map, reappeared in subsequent $2F_o - F_c$ maps, took part in at least one hydrogen-bonding interaction, and had temperature factors less than 80 Å^2. Regions of poor

Table 1: Crystallographic Data for Aerolysin Mutants

data	A300C	T253C	T253C/A300C
temp (K)	100	100	100
cell dimensions (*a*, *c*) (Å)	102.5, 216.2	102.4, 216.7	102.9, 217.7
max resolution (Å)	2.9	3.0	2.9
no. of crystals	1	1	1
total no. of observations	150635	132761	183708
no. of unique reflections	25034	20590	23208
completeness of data (%)[a]	96.1 (77.3)	86.2 (91.0)	87.7 (74.0)
no. of data $>3\sigma_I$ (%)[a]	66.8 (25.7)	62.5 (37.0)	69.8 (35.7)
I/σ_I	9.2 (2.4)	9.4 (3.0)	12.6 (3.8)
multiplicity	6.0	6.4	7.9
R_{merge} (%)[a,b]	14.3 (49.0)	12.9 (41.1)	11.3 (33.6)

[a] The values in parentheses are for the highest resolution bin (approximate interval of 0.5 Å). [b] $R_{merge} = \sum_{hkl}\sum_i|I_i - \langle I\rangle|/|\langle I\rangle|$, where I_i is the intensity for the *i*th measurement of an equivalent reflection with indices *h,k,l*.

Table 2: Refinement Statistics for Aerolysin Mutants

	A300C	T253C	T253C/A300C
non-hydrogen atoms			
protein	7051	7045	7037
solvent	81	68	82
resolution (Å)	15.0−2.9	15.0−3.0	15.0−2.9
$R_{conventional}$ (%)	24.1	23.2	24.0
R_{free} (%)	29.6	29.7	30.1
rmsds from ideal geometry			
bonds (Å)	0.008	0.008	0.008
angles (deg)	1.4	1.4	1.4
dihedrals (deg)	25.4	25.4	25.5
impropers (deg)	1.3	1.3	1.2
mean *B* (loop − mon. A) (Å^2)	57.1	76.7	41.5
mean *B* (loop − mon. B) (Å^2)	39.9	65.7	35.8
residues in most favorable regions of Ramachandran plot (%)	86.1	83.8	85.3

electron density were checked using omit maps in which the region of interest was first deleted from the model. Then a round of positional refinement was performed to minimize model bias, and a map was calculated from the resultant model. The final refinement statistics of the models are presented in Table 2. The *R*-factor values are typical for conservative models at modest resolution (*14*). A stereochemical analysis of the refined structures with the program PROCHECK (*15*) gave values either similar or better than those expected for structures refined at similar resolutions.

The starting model for the A300C mutant gave an *R*-factor of 33.4% (R_{free} = 33.3%) which reduced to 32.5% (R_{free} = 32.1%) after rigid-body refinement. After a round of positional refinement followed by grouped *B*-factor refinement, electron density maps were calculated. There was one significant peak of 4.4σ in the $F_{mutant} - F_{native}$ map adjacent to the Cβ atom of alanine 300 of the B monomer, thus confirming the mutation. At this stage, the alanine residues at position 300 were changed to cysteine residues, and a final cycle of positional refinement was run. The starting model for the T253C mutant gave an *R*-factor of 32.9% (R_{free} = 33.6%) which reduced to 31.8% (R_{free} = 32.9%) after rigid-body refinement. After a round of positional refinement followed by group *B*-factor refinement, electron density maps were calculated. There was one significant peak of 3.5σ in the $F_{mutant} - F_{native}$ map adjacent to the Cβ atom of threonine 253 in the B monomer, thus confirming the mutation. The threonine residues at position 253 were changed to cysteine residues, and the model was subjected to a final round of positional refinement. The likely reason why the peak height of the sulfur atom in the $F_{mutant} - F_{native}$ map of each single site mutant was higher for the B monomer is because of the lower mobility of the loop tip in this monomer due to crystal packing (Table 2).

The starting model for the T253C/A300C double mutant gave an *R*-factor of 39.3% (R_{free} = 39.5%) which reduced to 34.4% (R_{free} = 35.8%) after rigid-body refinement. After a round of positional refinement followed by group *B*-factor refinement, electron density maps were calculated. The largest peaks in the $F_{mutant} - F_{native}$ map of 4.3 and 6.6σ were located between the Cβ atoms of threonine 253 and alanine 300 in each monomer, thus confirming the double mutation. At this stage, the threonine and alanine residues were changed to cysteine residues, and a final round of positional refinement was performed.

Measurement of Binding and Oligomerization. Rat erythrocytes were used to follow binding and oligomerization using a modification of our published procedure (*6*). Briefly, 5×10^8 rat erythrocytes in 20 mM HEPES, 0.15 M NaCl, 0.3 M sucrose, 0.1% BSA, pH 7.4, were incubated with 10^{-7} M wild-type or mutant proaerolysin or aerolysin. Activation of proaerolysin involved treating 10^{-6} M proaerolysin with 2 μg/mL trypsin for 15 min at room temperature and then adding trypsin inhibitor to 10 μg/mL. Following incubation at 37 °C for 10 min, samples were centrifuged for 2 min at 10 000 rpm in a Beckman JA-17 rotor. Supernatants were removed, and the pellets were washed in the incubation buffer and recentrifuged. Pellets were finally resuspended in 240 μL of sample buffer, and the proteins were separated by SDS−PAGE and blotted. Aerolysin, proaerolysin, and the aerolysin heptamer were detected using a rabbit α-aerolysin polyclonal antibody.

Tryptophan Fluorescence and MIANS Labeling. Fluorescence measurements were carried out with a Photon

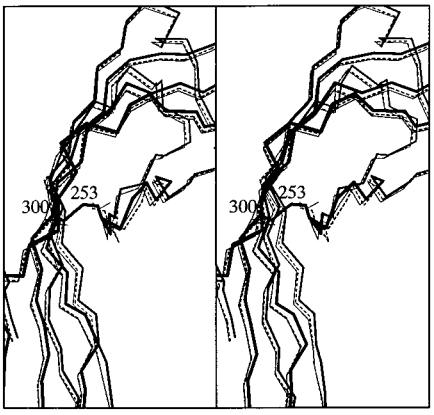

FIGURE 2: Superposition of the mutant structures in the region of domain 3. The T253C, A300C, and T253C/A300C mutants are shown in dashed, thin, and thick lines, respectively. The figure was generated with the program MOLSCRIPT (*21*).

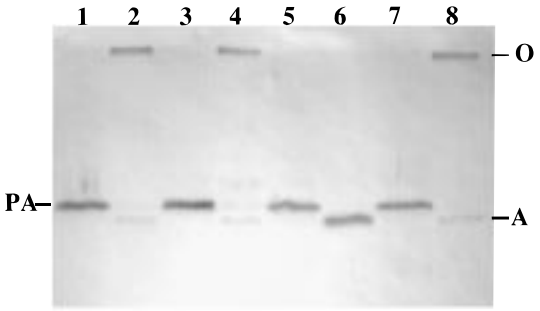

FIGURE 3: Binding and oligomerization of the cysteine mutants. Rat erythrocytes were incubated with the aerolysin or proaerolysin forms of wild-type or the mutant proteins. Samples were separated by SDS−PAGE, and blotted as described under Experimental Procedures. The positions of aerolysin (A), proaerolysin (PA), and the aerolysin oligomer (O) are shown. Lanes 1 and 2 contain membranes exposed to wild-type proaerolysin and aerolysin; lanes 3 and 4, T253C proaerolysin and aerolysin; lanes 5 and 6, T253C/A300C proaerolysin and aerolysin; lanes 7 and 8, A300C proaerolysin and aerolysin.

Technology International QM-1 spectrofluorometer equipped with a thermostated cuvette holder. For tryptophan fluorescence, the excitation and emission wavelengths were 295 and 340 nm, respectively. For MIANS, the excitation and emission wavelengths were 330 and 418 nm. Slit widths were 4 nm. MIANS labeling was performed at 30 °C in 150 mM NaCl, 20 mM Tris-HCl, pH 8.2, at a protein concentration of 0.12 μM. The probe was added in 10-fold molar excess. The stoichiometry of labeling was determined spectrophotometrically, using an extinction coefficient of 17 000 for MIANS at 327 nm.

Other Methods. Protein concentrations were based on an absorbency of 2.5 at 280 nm for a pure 1 mg/mL solution of the protoxin (*16*). Proaerolysin was activated as described in van der Goot *et al.* (*17*). SDS−PAGE was carried out as described by Neville (*18*).

RESULTS

Secretion and Purification of the Cysteine Mutants. All three cysteine proaerolysin mutants were secreted by *A. salmonicida*, and all of them could be purified to apparent homogeneity using our published procedure. They were each correctly processed by trypsin to produce a single product corresponding to aerolysin (see below). All mutants crystallized readily under similar conditions to wild-type protoxin, and the crystals appeared isomorphous with wild-type crystals.

Structure of A300C. This model is of good quality with a final *R*-factor of 24.1% (R_{free} = 29.6%) and good stereochemistry (Table 2). The electron density maps confirmed the mutation (data not shown), and the temperature factors for the loop region are comparable to those observed in the wild-type structure (Table 2 and unpublished results). Overall the mutant structure appears identical to the wild-type structure with one exception. Thr 253 has rotated away from the core of domain 3 to avoid steric clashes with the newly introduced cysteine (Figure 2). The cysteine side chain stacks against the edge of the aromatic ring of Phe 410.

Structure of T253C. The model for this mutant is also of good quality with a final *R*-factor of 23.2% (R_{free} = 29.7%) and good stereochemistry (Table 2). The positioning of the newly introduced cysteine residue was unambiguous due to the strong scattering of the sulfur atom. Superposition of this model on the wild-type structure indicated that the tip of the loop moves approximately 1 Å away from the β-sheet in domain 3. In the wild-type structure, Thr 253 is involved in a hydrogen bonding interaction, and the loss of this interaction has presumably led to the loop movement. The increased flexibility of the loop is reflected in the temperature factors (Table 2).

Structure of T253C/A300C. This mutant yielded a model with a final *R*-factor of 24.0% (R_{free} = 30.1%) and good stereochemistry (Table 2). The electron density within the region of the double mutation in both monomers clearly showed the formation of the disulfide bridge. The lower temperature factors for the loop in both monomers (Table 2) presumably result from the newly introduced covalent bond between the loop and the sheet in domain 3. Superposition of the dimer on the wild-type structure showed a small translational rigid-body shift of monomer A with respect to monomer B, causing a slight increase of about 0.5 Å in the monomer−monomer separation. This reflects small differences between the two monomers in the wild-type structure due to crystal packing forces (see below). Superposition of the A monomer over wild-type indicated that no significant movements of either main-chain or side-chain atoms had occurred. However, in the B monomer, the tip of the loop has moved approximately 1 Å in toward the β-sheet so as to allow the formation of the disulfide bridge. The domain 3's of each monomer in the double mutant are virtually superimposable.

Hemolytic Activity of the Cysteine Mutants. Both the T253C and A300C mutants were as active as wild-type aerolysin, whereas the double mutant had no detectable activity (not shown). The reason for this is apparent from the results in Figure 3. This is a Western blot developed with an anti-aerolysin antibody after SDS−PAGE separation of rat erythrocyte membranes which had been incubated with mutant or wild-type protoxins, or with the corresponding aerolysins produced by trypsin activation. It is apparent from the figure that all of the mutant proaerolysins bound to rat erythrocytes at about the same level as wild-type proaerolysin. As we have reported previously, wild-type aerolysin also bound to the cells, but it was converted to the oligomeric

Table 3: Hemolytic Titers of Culture Supernatants from *A. salmonicida* Grown in Normal Medium or Medium Containing DTT and Expressing Wild-Type Proaerolysin or the A300C-T253C Mutant

medium	proaerolysin	2 h induction titer	4 h induction titer
normal	wild type	7.5	10
normal	A300C-T253C	0	0
+DTT	wild type	5.5	8.5
+DTT	A300C-T253C	6.5	9

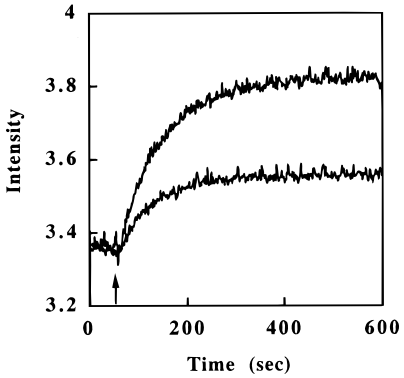

FIGURE 4: Changes in the tryptophan fluorescence of the double mutant A300C-T253C (lower curve) and wild-type proaerolysin (upper curve) upon activation. The arrow marks the time at which trypsin was added. See the text for details.

form during the incubation period (*6*). This was also the case for each of the single mutants. However, although the double mutant aerolysin also bound to the cells, no oligomer was detected (Figure 3). This leads to the conclusion that the new disulfide bridge that has formed locks the loop to the five-stranded sheet and prevents oligomerization.

Activation of the T253C/A300C Mutant under Reducing Conditions. If the new bridge alone is responsible for the inactivity of the double mutant, then the protein should be active when the bridge is reduced, or when it is prevented from forming. Reduction of the new bridge without denaturation proved to be very inefficient because it is buried within the protein. Thus, although the mutant toxin became hemolytic after incubation with dithiothreitol as predicted, it was far less active than wild type (data not shown).

We have shown that when *A. salmonicida* is grown under reducing conditions, disulfide bridges are not formed in the proteins it secretes. This gave us a way to produce the reduced double mutant in an unoxidized form so that we could test its activity. Bacteria expressing wild-type aerolysin or the double mutant were grown side by side in normal medium or in medium containing DTT. The titers of culture supernatants were then compared. The results are shown in Table 3. The supernatant containing the double mutant from cells grown without the reducing agent had no activity, whereas the activity of the supernatant from the cells grown with DTT was similar to the activity of wild type.

Changes in Tryptophan Fluorescence upon Activation of A300C-T253C and Wild-Type Proaerolysin. There is a pronounced change in the Trp fluorescence of proaerolysin when it is activated by trypsin, implying that there is a change in the structure of the protein (*19*). A similar change was observed for both the T253C and A300C mutants, but the results in Figure 4 show that the change was markedly lower for the double cysteine mutant, implying that the conformational change that normally accompanies activation is hindered.

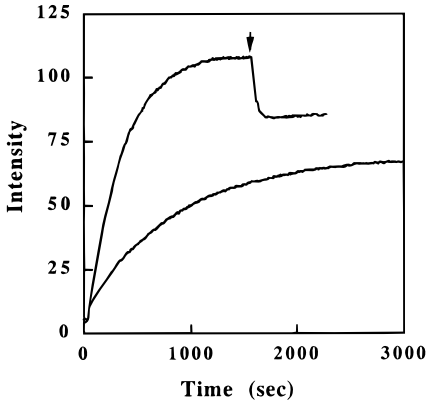

FIGURE 5: Comparison of MIANS labeling of A300C proaerolysin and aerolysin. MIANS labeling of A300C proaerolysin (upper curve) and aerolysin (lower curve) was followed as described under Experimental Procedures. The arrow marks the time at which trypsin was added to the proaerolysin sample.

Use of MIANS To Measure Changes in the Environment of 253C and 300C as a Result of Activation. The sulfhydryl-specific probe MIANS has a much higher quantum yield in a hydrophobic environment than in water, and it can therefore be a useful indicator of the environment of cysteines in proteins (*20*). The results in Figure 5 show that A300C proaerolysin reacted rapidly with the reagent and that there was a pronounced increase in fluorescence, an indication that the new cysteine is in a relatively hydrophobic environment, in agreement with the crystal structure of the A300C mutant (Figure 2). The environment of 300C was somewhat different in the aerolysin form of the mutant protein. Reaction with MIANS was slower, and the maximum fluorescence intensity was somewhat lower. The change in the environment of 300C could be observed directly as a decrease in fluorescence when A300C proaerolysin was activated by trypsin after it had reacted with MIANS (Figure 5). The reduction in emission intensity that accompanied activation indicates that the environment of 300C became more polar, which would result if the loop moves away from the sheet. No change in fluorescence intensity was observed if trypsin inhibitor was added before the addition of trypsin. Similar results were obtained with the T253C mutant, although the quantum yields of both forms of the protein were much lower than with A300C aerolysin and proaerolysin (data not shown). Wild-type proaerolysin and aerolysin did not react with MIANS under these conditions.

Analysis of fluorescence emission spectra of MIANS-labeled A300C proaerolysin and aerolysin confirmed a change in the environment of the cysteine upon activation. The results are shown in Figure 6. The maximum emission wavelength λ_{max} of MIANS reacted with β-mercaptoethanol is 447 nm. Upon reaction with A300C aerolysin, the maximal fluorescence intensity increased 4.4 fold, and λ_{max} underwent a strong blue shift to 430 nm. Finally, upon reaction with proaerolysin, the maximal MAINS fluorescence intensity increased 10-fold when compared to the intensity of the MIANS$-\beta$-mercaptoethanol complex and 2.3-fold when compared to aerolysin. A further 3 nm blue shift of λ_{max} was observed ($\lambda_{max} = 427$ nm).

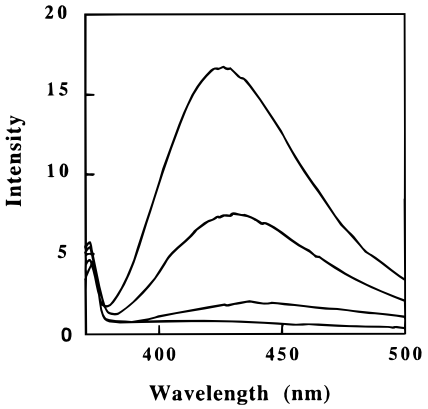

FIGURE 6: Fluorescence spectra of MIANS-labeled A300C proaerolysin (upper curve) and aerolysin (second curve from top). The spectra of MIANS alone (bottom curve) and MIANS−β-mercaptoethanol (second curve from bottom) are also shown. See the text for details.

DISCUSSION

The results of all of the experiments described in this study confirm our prediction that the loop in domain 3 of aerolysin must move away from the β-sheet for oligomerization to occur. We produced three mutant proteins, T253C, A300C, and the corresponding double mutant. The crystal structures of both the T253C and A300C proaerolysins confirmed the correct mutations and showed the residues at the tip of the loop to be highly mobile. This mobility would allow access of alkylating reagents to these buried residues, accounting for the reactivity we observed with MIANS. Alkylation of either residue with MIANS, or other reagents we tried, such as acrylodan and iodoacetamide, did not have any effect on hemolytic activity, suggesting neither residue resides in the bilayer upon membrane insertion of the aerolysin heptamer, in agreement with our model of the channel structure (*2*).

The crystal structure of the double mutant, T253C/A300C, confirmed that the disulfide bridge was formed between residues 253 and 300 as we predicted it would be. The introduction of the bridge tied down the loop tip, hence reducing its mobility as judged by the low temperature factors in this region of both monomers (Table 2). This mutant was secreted normally in a completely oxidized, inactive state, and it was found difficult to reduce using either mercaptoethanol or DTT. This can be explained by the fact that the bridge is completely buried in the crystal structure (Figure 2). However, the protein was active when expressed in bacteria growing in DTT, confirming that the inactivity of the oxidized form was not due to the double mutation *per se*.

Our results indicate that the bridge locking the loop to the β-sheet inactivates the protein at a step that follows activation. Thus, the double mutant bound to rat erythrocytes in the same way as wild-type, and it was correctly processed by trypsin. Although the interpretation of fluorescence measurements may be complex, the results of MIANS reactivity experiments, and the comparison of the changes in tryptophan fluorescence of wild type and the double mutant that accompany activation, strongly suggest that inactivity is due to failure of the loop in domain 3 to move away from the five-stranded β-sheet after activation. This prevents the formation of insertion-competent oligomers and hence blocks channel formation.

ACKNOWLEDGMENT

We thank Angela Schulze and Tracy Lawrence for their skilled technical assistance.

REFERENCES

1. Parker, M. W., van der Goot, F. G., and Buckley, J. T. (1996) *Mol. Microbiol. 19*, 205−212.
2. Parker, M. W., Buckley, J. T., Postma, J. P. M., Tucker, A. D., Leonard, K., Pattus, F., and Tsernoglou, D. (1994) *Nature 367*, 292−295.
3. Song, L., Hobaugh, M. R., Shustak, C., Cheley, S., Bayley, H., and Gouaux, J. E. (1996) *Science 274*, 1859−1866.
4. Petosa, C., Collier, R. J., Klimpel, K. R., Leppla, S. H., and Liddington, R. C. (1997) *Nature 385*, 833−838.
5. Hazes, B., and Dijkstra, B. W. (1988) *Protein Eng. 2*, 119−126.
6. Green, M. J., and Buckley, J. T. (1990) *Biochemistry 29*, 2177−2180.
7. Buckley, J. T., Wilmsen, H. U., Lesieur, C., Schulze, A., Pattus, F., and Parker, M. W. (1995) *Biochemistry 34*, 16450−16455.
8. Wong, K. R., McLean, D. M., and Buckley, J. T. (1990) *J. Bacteriol. 5*, 2745−2751.
9. Buckley, J. T. (1990) *Biochem. Cell Biol. 68*, 221−224.
10. Tucker, A. D., Parker, M. W., Tsernoglou, D., and Buckley, J. T. (1990) *J. Mol. Biol. 212*, 561−562.
11. Otwinowski, Z. (1993) in *Data Collection and Processing* (Sawyer, L., Isaacs, N., and Bailey, S., Eds.) pp 56−62, SERC Daresbury Laboratory, Warrington, U.K.
12. CCP4 Suite (1994) *Acta Crystallogr. D50*, 750−763.
13. Brünger, A. T. (1993) *X-PLOR: A system for X-ray Crystallography and NMR*, Department of Molecular Biophysics and Biochemistry, Yale University, New Haven, CT.
14. Kleywegt, G. J., and Jones, T. A. (1995) *Structure 3*, 535−540.
15. Laskowski, R. A., McArthur, M. W., Moss, D. S., and Thorton, J. M. (1993) *J. Appl. Crystallogr. 26*, 282−291.
16. van der Goot, F. G., Hardie, K. R., Parker, M. W., and Buckley, J. T. (1994) *J. Biol. Chem. 269*, 30496−30501.
17. van der Goot, F. G., Pattus, F., Wong, K. R., and Buckley, J. T. (1993) *Biochemistry 32*, 2636−2642.
18. Neville, D. M. (1971) *J. Biol. Chem. 246*, 6328−6334.
19. van der Goot, F. G., Lakey, J., Pattus, F., Kay, C. M., Sorokine, O., Dorsselaer, A. V., and Buckley, J. T. (1992) *Biochemistry 31*, 8566−8570.
20. Haugland, R. P. (1989) in *Handbook of Fluorescent Probes and Research Chemicals*, p 25, Molecular Probes Inc., Eugene, OR.
21. Kraulis, P. (1991) *J. Appl. Crystallogr. 24*, 946−950.

BI9721039